

Rydberg Interaction-Induced Distortion of the Autler–Townes Spectra in Cold Lithium Atoms

Sergey Saakyan , Nikita Morozov, Vladimir Sautenkov and Boris B. Zelener

Joint Institute for High Temperatures of the Russian Academy of Sciences, Izhorskaya 13 Bldg 2, Moscow 125412, Russia

* Correspondence: saakyan@ihed.ras.ru

Abstract: In this article, effects of the strong long-range interaction of Rydberg atoms on the Autler–Townes splitting spectrum are investigated. Preliminary results are obtained for various excitation times and Rydberg atom densities. The $2S_{1/2}$ and $2P_{1/2}$ levels of lithium-7 are coupled with strong laser field and probed by another laser via excitation into a 70S Rydberg level. Interactions between Rydberg atoms excited by the probe beam lead to the broadening of the Autler–Townes spectra. At high concentrations of Rydberg atoms, a suppression of the excitation of the Autler–Townes peak at red detuning is observed.

Keywords: Rydberg atoms; magneto-optical trap; Autler–Townes splitting; lithium

1. Introduction

Strong long-range interaction between Rydberg atoms modifies properties and behavior of a dense ensemble of Rydberg atoms. These interactions can be used in quantum information processes [1–3], in dynamically driven dissipative systems [4] and in a wide range of many-body physics phenomena. Rydberg atoms of lithium are proposed as an object for the study of Rydberg dressing phenomena [5]. For imaging of cold ions, large polarizability of Rydberg atoms is used [6].

Nonlinear optical effects such as Autler–Townes (AT) splitting [7] and electromagnetically induced transparency (EIT) have been studied in strongly interacting cold [8] and hot [9,10] atomic samples. In [11,12], the ground level and the first excited level of cesium are coupled by a strong field and are probed via excitation into a Rydberg level. Interaction between Rydberg atoms results in sufficient broadening of the AT spectra. The population redistribution of Rydberg states caused by blackbody radiation (BBR) [13,14] and Rydberg–Rydberg collisions [15] together with direct photoionization by BBR results in appearance of charged particles in the excitation volume. Many effects exist which are associated with charged particles and with formation of ultracold plasma in a cold gas of Rydberg atoms, such as ion blockade or antiblockade of excitation [16] and avalanche ionization of the dense Rydberg gas [17,18]. This interaction-induced dephasing increases the critical coupling power above which AT splitting occurs.

In [14], it was found for the nS lithium series that the rate of population of high Rydberg levels by blackbody radiation abnormally depends on n . This anomaly is analogous to the occurrence of the Cooper minimum in a discrete spectrum [14]. The rate of direct photoionization by blackbody radiation for the nS states of lithium is more than an order of magnitude less than that of potassium and caesium.

In a three-level system with a long-lived metastable intermediate level, the AT splitting is observed under conditions similar to the EIT conditions in a traditional three-level cascade system of alkali metal atoms. This type of three-level systems was studied in [19] by means of atoms of alkaline-earth strontium. Long-range interaction between Rydberg atoms results in strong decoherence, shifting and deformation of the observed AT spectra.



Citation: Saakyan, S.; Morozov, N.; Sautenkov, V.; Zelener, B.B. Rydberg Interaction-Induced Distortion of the Autler–Townes Spectra in Cold Lithium Atoms. *Atoms* **2023**, *11*, 73. <https://doi.org/10.3390/atoms11040073>

Academic Editors: J. Tito Mendonca, Hugo Terças and James F. Babb

Received: 18 November 2022

Revised: 5 April 2023

Accepted: 11 April 2023

Published: 13 April 2023



Copyright: © 2023 by the authors. Licensee MDPI, Basel, Switzerland. This article is an open access article distributed under the terms and conditions of the Creative Commons Attribution (CC BY) license (<https://creativecommons.org/licenses/by/4.0/>).

In this article, we study the effects of the strong long-range interaction of Rydberg atoms on the Autler–Townes splitting spectrum. Lithium D1 line transitions are strongly coupled and probed via excitation into 70S Rydberg states. Interactions between Rydberg atoms excited by means of a probe beam result in the broadening of the Autler–Townes spectra. At high concentrations of Rydberg atoms, significant suppression of the excitation of the AT peak at red detuning is observed.

2. Experimental Setup and Methods

For cooling and trapping atoms in a magneto-optical trap (MOT), we use two amplified external-cavity diode lasers (wavelength 671 nm) working at the D2 line transitions of lithium-7. The main cooling laser is locked at the saturation absorption resonance in a high temperature vapor cell (D2 line transition $2S_{1/2}(F = 2) \rightarrow 2P_{3/2}(F' = 3)$, Figure 1a). We use a fused silica heat-pipe oven with lithium [20]. A molybdenum foil is placed in the middle of the fused silica tube in the heating area. In order to observe good locking signals, the cell is heated up to 400 °C [21]. In order to avoid deposition of lithium onto the windows, we use argon at pressure 0.01 Torr as a buffer gas. The quartz gas cell with cold windows has been used for more than ten years without outgassing or repair. The second cooling laser is stabilized around the transition $2S_{1/2}(F = 1) \rightarrow 2P_{3/2}(F' = 2)$ using the optical beat-note signal between cooling lasers by means of the frequency offset locking technique [22]. Our MOT is formed by three pairs of counter-propagating circularly polarized beams. The intensity of the MOT beams is controlled by an acousto-optical modulator. Other details of the cooling and trapping of lithium-7 are described elsewhere [23,24]. We confine $N_0 = 3(1) \times 10^8$ atoms with the peak density $n \approx 10^{11} \text{ cm}^{-3}$. The temperature of cold atoms in the working MOT is measured via the differential two-photon spectroscopic technique, and for our MOT parameters is equal to 0.8 mK [23,25].

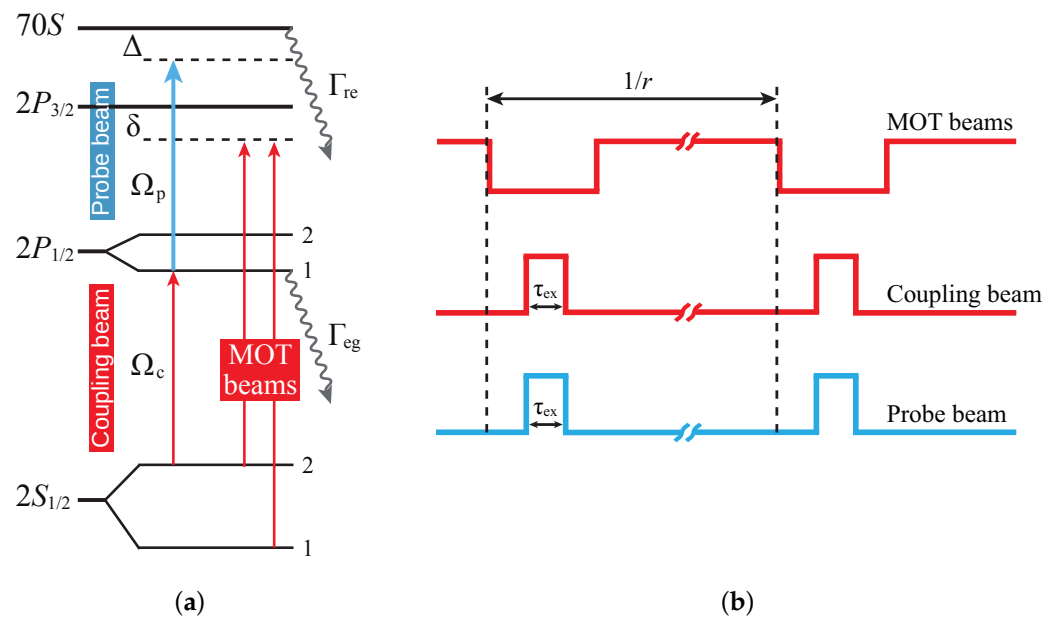


Figure 1. (a) Relevant level scheme in ^7Li . (b) Excitation time sequence. Here r is the pulse repetition rate, τ_{ex} is duration of the coupling and probe beams. The relative timings between pulses are not in scale.

Hyperfine levels in the D2 line are closely spaced and are not completely resolved [26]. Separation between the hyperfine levels is comparable to the natural linewidths of the D2 line components $2\pi \times 6 \text{ MHz}$. Closely spaced hyperfine states in the D2 line make it less preferable for studies of such coherent effects as Autler–Townes splitting or EIT [27]. For clearer observation of the AT splitting, the $2S_{1/2}$ and $2P_{1/2}$ levels of lithium-7 are coupled in our study with a strong laser field. The distance between the D1 line and D2

line of the lithium-7 exceeds 10 GHz [26]. For the coupling beam, an additional diode laser with a wavelength of 671 nm is used, which was frequency locked by saturated absorption resonances in a high temperature vapor cell. To drive the $2P_{1/2}$ -70S transition, a UV laser system (with wavelength 350 nm) is used [28]. The laser frequency is locked to a temperature-stabilized reference cavity.

Both the probe beam and the coupling beam are spatially filtered by means of single-mode polarization maintaining fibers and are focused to the center of the MOT. The waist of the probe beam and of the coupling beam are 60(10) μm and 250(15) μm , respectively, and are measured by charge-coupled device camera. In all experiments, the Rabi frequency of the probe beam is much lower than the Rabi frequency of the coupling beam and is equal to $\Omega_p = 2\pi \times 0.4$ MHz [29]. The atomic cloud in the MOT has a Gaussian distribution with a diameter equal to 1.7(2) mm at the $1/e$ level. The overlap between the atom cloud and the probe beam forms the effective volume in which Rydberg atoms are excited and which is equal to $V = 10(2) \times 10^{-6}$ cm³. The strong laser coupling of the transition produces an AT doublet of dressed states. Separation between these two new energy levels is often used for determining the effective intensity of the coupling beam. This method makes it possible to precisely determine the intensity of the radiation seen via the atomic sample. Direct calculation of the Rabi frequency by means of the measured optical power leads to large uncertainties associated with the overlapping between waists of the probe beam and the coupling beam. In our case, we evaluate this relative error as approximately 30–40%.

The coupling beam and the probe beam have linear parallel polarization and drive $2S_{1/2}(F = 2)$ - $2P_{1/2}(F' = 1)$ and $2P_{1/2}(F' = 1)$ -70S transitions, respectively. Experimental cycles are repeated with the variable rate r . The pump beam and the probe beam with duration τ_{ex} are switched on simultaneously, a few microseconds after turning off the MOT beams. The pulse sequences of our experiment are shown in Figure 1b. We observe the trap loss spectrum by means of scanning the probe laser near the Rydberg transition frequency and by simultaneously applying excitation pulses with repetition rate r .

We find the number of Rydberg atoms produced in each excitation cycle by means of a model of simple rate equation (RE). The fluorescence signal is proportional to the number of atoms N in the trap. The simplified dynamics of the trapped atoms in the MOT $N(t)$ with constant loading rate R may be described by the following equation

$$\frac{dN(t)}{dt} = R - \Gamma N(t), \tag{1}$$

which has the following solution $N(t) = N_0(1 - e^{-\Gamma t})$, where the loss $\Gamma = \Gamma_{\text{col}} + \Gamma_{\text{ex}}^{\text{eff}}$ is described by the sum of collisional losses of neutral atoms due to their collisions with the residual gas in the vacuum chamber and losses due to the excitation of neutral atoms to Rydberg states. Without the coupling beam and the probe beam, $\Gamma_{\text{ex}}^{\text{eff}} = 0$, and the stationary number of atoms $N_0 = R/\Gamma_{\text{col}}$. In our MOT, $R/N_0 = 0.056$ s⁻¹ and the collisional loss is $\Gamma_{\text{col}} = 1/\tau_{\text{col}} = 1/18$ s⁻¹. In cases where the number of excited atoms in one cycle is sufficiently small, the effective losses upon excitation can be represented as $\Gamma_{\text{ex}}^{\text{eff}} = \Gamma_{\text{ex}}\tau_{\text{ex}}r$. From the stationary solution of Equation (1), we obtain the expression

$$\Gamma_{\text{ex}}^{\text{eff}} = \Gamma_{\text{col}} \left(\frac{N_0}{N_{\text{st}}} - 1 \right), \tag{2}$$

where N_{st} is the stationary number of trapped atoms in the presence of excitation pulses having the repetition rate r . The number of Rydberg atoms excited in a one pulse cycle with duration τ_{ex} can be obtained as $N_r = N_0\Gamma_{\text{ex}}\tau_{\text{ex}}$.

By means of applying a strong laser field between the ground state and the intermediate state, we generate two separated Autler–Townes peaks. Following the model considered in [11,12,30] for our cascade excitation scheme, the Hamiltonian in the rotating-wave approximation can be expressed as follows

$$H = \frac{\hbar}{2} \begin{pmatrix} 0 & \Omega_c & 0 \\ \Omega_c & 0 & \Omega_p \\ 0 & \Omega_p & -2\Delta \end{pmatrix}. \quad (3)$$

Density matrix evolution is described by the Lindblad equation

$$\dot{\rho} = -\frac{i}{\hbar}[H, \rho] + \mathcal{L}, \quad (4)$$

where decay and Rydberg-induced dephasing are included in the Liouville operator [12]

$$\mathcal{L} = \begin{pmatrix} \Gamma_{eg}\rho_{22} & -\frac{1}{2}\gamma_2\rho_{12} & -\frac{1}{2}\gamma_3\rho_{13} \\ -\frac{1}{2}\gamma_2\rho_{21} & -\Gamma_{eg}\rho_{22} + \Gamma_{re}\rho_{33} & -\frac{1}{2}(\gamma_2 + \gamma_3)\rho_{23} \\ -\frac{1}{2}\gamma_3\rho_{31} & -\frac{1}{2}(\gamma_2 + \gamma_3)\rho_{32} & -\Gamma_{re}\rho_{33} \end{pmatrix}. \quad (5)$$

Here $\gamma_2 = \gamma_e + \Gamma_{eg}$ is the dephasing rate of the $2P_{1/2}(F' = 1)$ level which is equal to the natural linewidth of the $2P_{1/2}$ level $\Gamma_{eg} = 2\pi \times 6$ MHz, other decay processes of this state can be neglected, and $\gamma_3 = \gamma_r + \Gamma_{re}$ is the dephasing rate of the Rydberg state. The natural width of the Rydberg state Γ_{re} is sufficiently small, in our case $\Gamma_{re} \ll \gamma_r$. The probe beam excites the high-lying 70S Rydberg state, with strong van der Waals interaction (dispersion coefficient $C_6 = -585$ GHz μm^6 [31]). This results in the large values of the Rydberg dephasing rate, and here we consider $\gamma_3 \approx \gamma_r$.

In the stationary case, the imaginary part $\text{Im}(\rho_{23})$ is proportional to the absorption of the probe beam and to the loss of atoms measured in our experiment [11,30]:

$$\text{Im}(\rho_{23}) \propto \frac{\gamma_2(\gamma_3^2 + 4\Delta^2) + \gamma_3|\Omega_c|^2}{|(\gamma_2 + 2i\Delta)(\gamma_3 + 2i\Delta) + \Omega_c^2|^2}. \quad (6)$$

The eigenvalues corresponding to the Hamiltonian (3) can be written as $E_{\pm} \approx \pm\hbar\Omega_c/2$. According to this model, we can experimentally determine the Rabi frequency of the coupling beam by means of measuring separation between the AT peaks.

3. Results

The two-step $2S_{1/2}$ - $2P_{1/2}$ -70S transition spectra for a low Rabi frequency of the coupling field $\Omega_c \ll \Gamma_{eg}$ are presented in Figure 2 (blue line). This spectral dependence is well approximated by the Lorentzian distribution with full width at half maximum FWHM = 10.8 MHz (the dashed line in Figure 2). We use this value in Equation (6) as the experimental value of the intermediate-level dephasing coefficient γ_2 in order to take into account the Doppler broadening and other possible dephasing mechanisms.

The red curve in Figure 2 shows the spectral dependence in cases where the $2S_{1/2}$ and $2P_{1/2}$ levels of lithium-7 are coupled with a strong laser field and are probed by another laser via excitation into a 70S Rydberg level. For short excitation timescale $\tau_{ex} = 100$ ns and for a small number of Rydberg atoms, AT peaks have equal amplitude. The symmetric AT peaks are in good agreement with the theoretical model (6) that takes dephasing into account. Interaction between Rydberg atoms results in sufficient broadening of the AT spectra. This interaction-induced dephasing eliminates the AT splitting (the peak separation from Figure 2 is $\Omega_c^{AT} = 2\pi \times 34$ MHz) and increases the critical coupling power above which the AT splitting occurs [12]. The Rabi frequency determined from intensity of the coupling beam is equal to $\Omega_c^{exp} = 2\pi \times 52(20)$ MHz. The indicated uncertainties are associated with the overlap between intensity distributions of the coupling beam and the probe beam in the excitation region.

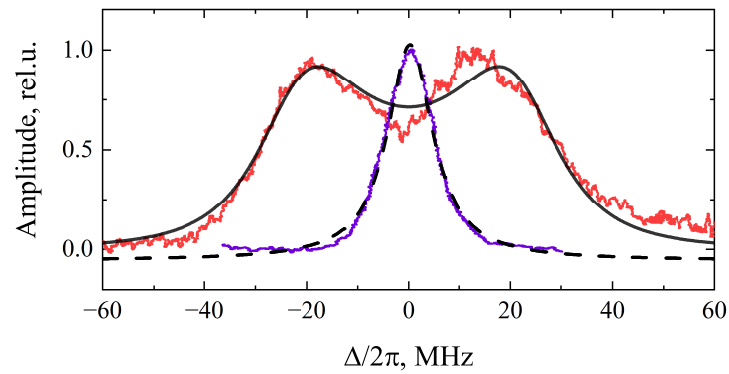


Figure 2. Two-step $2S_{1/2}-2P_{1/2}-70S$ transition spectra for the low Rabi frequency (blue curve) and the high Rabi frequency (red curve) of the coupling beam. The dashed curve is the best fit by means of a Lorentzian distribution with full width at half maximum FWHM = 10.8 MHz; the black solid curve is the best fit by means of Equation (6) with the dephasing rate $\gamma_3 = 2\pi \times 43$ MHz and $\Omega_c = 2\pi \times 47$ MHz. The separation of AT peaks (the distance between two maximum values) is $\Omega_c^{AT} = 2\pi \times 34$ MHz, and the measured Rabi frequency determined from intensity of the coupling beam is $\Omega_c^{exp} = 2\pi \times 52(20)$ MHz.

Interaction between Rydberg atoms excited by probe beams results in sufficient broadening of the AT peaks, and in their dramatic change. The potential of the long-range van der Waals interaction for a pair of Rydberg atoms at a distance R is equal to $U = -C_6/R^6$. The dispersion coefficient C_6 grows as the effective principal quantum number grows as n^{11} . The dephasing rate increases with effective quantum number n increasing or with the density of Rydberg atoms increasing. Figure 3a,b show the AT spectrum for two different values of the coupling beam power and for the same excitation pulse length $\tau_{ex} = 100$ ns. For a lower coupling beam power ($\Omega_c = 2\pi \times 34$ MHz), the peak number of Rydberg atoms excited in each pulse sequence does not exceed 10^3 . For a higher coupling beam power, as shown in Figure 3b, or for longer excitation time, as shown in Figure 3c, increasing the number of Rydberg atoms results in suppression of the AT peak compared to the peak observed for blue detuning of the probe beam Δ . Figure 3d,e correspond to the same coupling beam power and to different excitation times, $\tau_{ex} = 3 \mu s$ and $20 \mu s$, respectively. The strong interaction between Rydberg atoms changes the separation between the AT peaks, rather than the shape of the AT peaks only. The peak number of Rydberg atoms in Figure 3e corresponds to a density of approximately $1.4(2) \times 10^9 \text{ cm}^{-3}$. The corresponding long-range interaction for such density is equal to $U \approx 40(15)$ MHz. The RE model (1) does not take into account the temperature expansion of Rydberg atoms or other decay processes. The number of Rydberg atoms for excitation times longer than a few microseconds can be determined with a significant error.

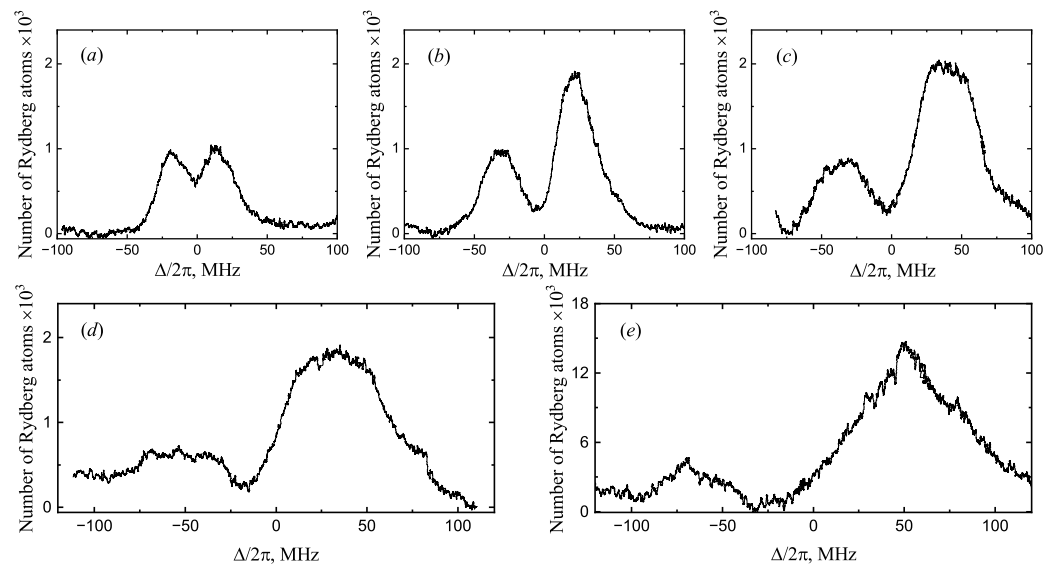


Figure 3. Number of Rydberg atoms excited by application of single pulse with duration τ_{ex} vs. probe beam detuning Δ : (a) $\Omega_{\text{c}}^{\text{AT}} = 2\pi \times 34$ MHz, $\Omega_{\text{c}}^{\text{exp}} = 2\pi \times 52$ MHz, $\tau_{\text{ex}} = 0.1$ μs ; (b) $\Omega_{\text{c}}^{\text{AT}} = 2\pi \times 54$ MHz, $\Omega_{\text{c}}^{\text{exp}} = 2\pi \times 71$ MHz, $\tau_{\text{ex}} = 0.1$ μs ; (c) $\Omega_{\text{c}}^{\text{AT}} = 2\pi \times 73$ MHz, $\Omega_{\text{c}}^{\text{exp}} = 2\pi \times 71$ MHz, $\tau_{\text{ex}} = 0.2$ μs ; (d) $\Omega_{\text{c}}^{\text{AT}} = 2\pi \times 81$ MHz, $\Omega_{\text{c}}^{\text{exp}} = 2\pi \times 97$ MHz, $\tau_{\text{ex}} = 3$ μs ; (e) $\Omega_{\text{c}}^{\text{AT}} = 2\pi \times 119$ MHz, $\Omega_{\text{c}}^{\text{exp}} = 2\pi \times 97$ MHz, $\tau_{\text{ex}} = 20$ μs . The frequencies $\Omega_{\text{c}}^{\text{AT}}$ are determined by the separation of AT peaks. The measured Rabi frequencies $\Omega_{\text{c}}^{\text{exp}}$ are determined from intensity of the coupling beam.

4. Conclusions and Outlook

In this article, the effects of the strong long-range interaction of Rydberg atoms on the Autler–Townes splitting spectrum are studied. Lithium D1 line transitions are strongly coupled and they are probed by means of excitation into 70S Rydberg states. Interactions between Rydberg atoms excited by the probe beam lead to broadening of the Autler–Townes spectra. At high concentrations of Rydberg atoms, suppression of the excitation of the AT peak at red detuning is observed. Significant distortions of the AT spectrum have been previously observed in alkaline-earth strontium [19]. These results for short excitation times are in good agreement with the mean-field models. However, like in [19], a dephasing source exists at longer excitation times that has not yet been described via the mean-field model. A significant difference exists between the cascade excitation scheme presented in this article and the scheme involving a metastable intermediate level. However, in our opinion, a possible reason for the high dephasing rate may be common. For nS lithium states, all the effects associated with BBR differ from the effects of other alkaline and alkaline-earth species. These experimental results can help in the correct interpretation of coherent effects in a strongly interacting gas.

For correct quantitative analysis, it is necessary to create a comprehensive model which should include density distribution and density variation during the pulse sequence. In future, we plan to systematically measure the AT spectrum using a charged particle detection system and the selective field ionization technique. This will allow us to measure BBR-induced redistribution of Rydberg states to obtain sufficient information about the behavior of a strongly interacting Rydberg system. We plan to reduce the uncertainties concerning the determination of the excitation volume and concerning the estimation of the Rydberg density. This will help us to take interactions into account and to create a correct model for explanation of our results.

Author Contributions: Conceptualization, S.S.; formal analysis, S.S., V.S., N.M. and B.B.Z.; visualization, S.S.; methodology, S.S.; validation, S.S. and N.M.; writing—original draft preparation, S.S.; writing—review and editing, S.S., N.M., V.S. and B.B.Z.; investigation, S.S.; software, N.M.; project administration, B.B.Z.; resources, B.B.Z.; funding acquisition, S.S. and B.B.Z. All authors have read and agreed to the published version of the manuscript.

Funding: The research was supported by the Russian Science Foundation Grant No. 19-72-00099 in the part of experiments and by the Ministry of Science and Higher Education of the Russian Federation (state assignment No. 075-01129-23-00) and the Grants Council of the President of the Russian Federation for state support of young scientists in Russia (grant MK-3869.2022.1.2) in the part of theoretical calculations.

Institutional Review Board Statement: Not applicable.

Informed Consent Statement: Not applicable.

Data Availability Statement: The data presented in this study are available on request from the corresponding author.

Conflicts of Interest: The authors declare no conflict of interest.

Abbreviations

The following abbreviations are used in this manuscript:

AT	Autler–Townes
BBR	Blackbody radiation
EIT	Electromagnetically induced transparency
FWHM	Full width at half maximum
MOT	Magneto-optical trap
RE	Rate equation
UV	Ultraviolet

References

- Adams, C.S.; Pritchard, J.D.; Shaffer, J.P. Rydberg atom quantum technologies. *J. Phys. B At. Mol. Opt. Phys.* **2019**, *53*, 012002. [\[CrossRef\]](#)
- Cheinet, P.; Pham, K.L.; Pillet, P.; Beterov, I.I.; Ashkarin, I.N.; Tretyakov, D.B.; Yakshina, E.A.; Entin, V.M.; Ryabtsev, I.I. Three-body Förster resonance of a new type in Rydberg atoms. *Quantum Electron.* **2020**, *50*, 213–219. [\[CrossRef\]](#)
- Yakshina, E.A.; Tretyakov, D.B.; Entin, V.M.; Beterov, I.I.; Ryabtsev, I.I. Observation of the Dipole Blockade Effect in Detecting Rydberg Atoms by the Selective Field Ionization Method. *J. Exp. Theor. Phys.* **2020**, *130*, 170–182. [\[CrossRef\]](#)
- Letscher, F.; Thomas, O.; Niederprüm, T.; Fleischhauer, M.; Ott, H. Bistability versus metastability in driven dissipative Rydberg gases. *Phys. Rev. X* **2017**, *7*, 021020. [\[CrossRef\]](#)
- Wüster, S.; Ates, C.; Eisfeld, A.; Rost, J.M. Excitation transport through Rydberg dressing. *New J. Phys.* **2011**, *13*, 073044. [\[CrossRef\]](#)
- Gross, C.; Vogt, T.; Li, W. Ion imaging via long-range interaction with Rydberg atoms. *Phys. Rev. Lett.* **2020**, *124*, 053401. [\[CrossRef\]](#) [\[PubMed\]](#)
- Piotrowicz, M.J.; MacCormick, C.; Kowalczyk, A.; Bergamini, S.; Beterov, I.I.; Yakshina, E.A. Measurement of the electric dipole moments for transitions to rubidium Rydberg states via Autler–Townes splitting. *New J. Phys.* **2011**, *13*, 093012. [\[CrossRef\]](#)
- Günter, G.; Robert-de-Saint-Vincent, M.; Schempp, H.; Hofmann, C.S.; Whitlock, S.; Weidemüller, M. Interaction enhanced imaging of individual Rydberg atoms in dense gases. *Phys. Rev. Lett.* **2012**, *108*, 013002. [\[CrossRef\]](#)
- Anderson, D.A.; Miller, S.A.; Raithel, G.; Gordon, J.A.; Butler, M.L.; Holloway, C.L. Optical measurements of strong microwave fields with Rydberg atoms in a vapor cell. *Phys. Rev. Appl.* **2016**, *5*, 034003. [\[CrossRef\]](#)
- Duarte Gomes, N.; da Fonseca Magnani, B.; Massayuki Kondo, J.D.; Marcassa, L.G. Polarization Spectroscopy Applied to Electromagnetically Induced Transparency in Hot Rydberg Atoms Using a Laguerre–Gaussian Beam. *Atoms* **2022**, *10*, 58. [\[CrossRef\]](#)
- Zhang, H.; Wang, L.; Chen, J.; Bao, S.; Zhang, L.; Zhao, J.; Jia, S. Autler–Townes splitting of a cascade system in ultracold cesium Rydberg atoms. *Phys. Rev. A* **2013**, *87*, 033835. [\[CrossRef\]](#)
- Zhang, H.; Zhang, L.; Wang, L.; Bao, S.; Zhao, J.; Jia, S.; Raithel, G. Autler–Townes spectroscopy with interaction-induced dephasing. *Phys. Rev. A* **2014**, *90*, 043849. [\[CrossRef\]](#)
- Beterov, I.I.; Ryabtsev, I.I.; Tretyakov, D.B.; Entin, V.M. Quasiclassical calculations of blackbody-radiation-induced depopulation rates and effective lifetimes of Rydberg nS , nP , and nD alkali-metal atoms with $n \leq 80$. *Phys. Rev. A* **2009**, *79*, 052504. [\[CrossRef\]](#)
- Beterov, I.I.; Ryabtsev, I.I.; Tretyakov, D.B.; Bezuglov, N.N.; Ekers, A. Ionization of nS , nP , and nD lithium, potassium, and cesium Rydberg atoms by blackbody radiation. *J. Exp. Theor. Phys.* **2008**, *107*, 20–27. [\[CrossRef\]](#)

15. Amthor, T.; Reetz-Lamour, M.; Westermann, S.; Denskat, J.; Weidemüller, M. Mechanical effect of van der Waals interactions observed in real time in an ultracold Rydberg gas. *Phys. Rev. Lett.* **2007**, *98*, 023004. [[CrossRef](#)]
16. Bounds, A.D.; Jackson, N.C.; Hanley, R.K.; Bridge, E.M.; Huillery, P.; Jones, M.P.A. Coulomb anti-blockade in a Rydberg gas. *New J. Phys.* **2019**, *21*, 053026. [[CrossRef](#)]
17. Robert-de Saint-Vincent, M.; Hofmann, C.S.; Schempp, H.; Gunter, G.; Whitlock, S.; Weidemüller, M. Spontaneous avalanche ionization of a strongly blockaded Rydberg gas. *Phys. Rev. Lett.* **2013**, *110*, 045004. [[CrossRef](#)]
18. Siercke, M.; Oon, F.E.; Mohan, A.; Wang, Z.W.; Lim, M.J.; Dumke, R. Density dependence of the ionization avalanche in ultracold Rydberg gases. *Phys. Rev. A* **2014**, *89*, 022701. [[CrossRef](#)]
19. DeSalvo, B.J.; Aman, J.A.; Gaul, C.; Pohl, T.; Yoshida, S.; Burgdörfer, J.; Hazzard, K.R.A.; Dunning, F.B.; Killian, T.C. Rydberg-blockade effects in Autler–Townes spectra of ultracold strontium. *Phys. Rev. A* **2016**, *93*, 022709. [[CrossRef](#)]
20. Vidal, C.R.; Cooper, J. Heat-Pipe Oven: A New, Well-Defined Metal Vapor Device for Spectroscopic Measurements. *J. Appl. Phys.* **1969**, *40*, 3370–3374. [[CrossRef](#)]
21. Olivares, I.E.; Gonzalez, I.A. Diode laser absorption spectroscopy of lithium isotopes. *Appl. Phys. B* **2016**, *122*, 1–7. [[CrossRef](#)]
22. Schünemann, U.; Engler, H.; Grimm, R.; Weidemüller, M.; Zielonkowski, M. Simple scheme for tunable frequency offset locking of two lasers. *Rev. Sci. Instrum.* **1999**, *70*, 242–243. [[CrossRef](#)]
23. Sautenkov, V.A.; Saakyan, S.A.; Bobrov, A.A.; Vilshanskaya, E.V.; Zelener, B.B.; Zelener, B.V. Differential two-photon spectroscopy for nondestructive temperature measurements of cold light atoms in a magneto-optical trap. *J. Opt. Soc. Am. B* **2018**, *35*, 1546–1551. [[CrossRef](#)]
24. Sautenkov, V.A.; Saakyan, S.A.; Bobrov, A.A.; Kudrinskiy, D.A.; Vilshanskaya, E.V.; Zelener, B.B. Optical Dipole Trap for Laser-Cooled Lithium-7 Atoms. *J. Russ. Laser Res.* **2019**, *40*, 230–236. [[CrossRef](#)]
25. Bobrov, A.A.; Saakyan, S.A.; Sautenkov, V.A.; Vilshanskaya, E.V.; Zelener, B.V.; Zelener, B.B. Determination of characteristics of a magneto-optical trap by the spectral width of coherent two-photon resonance. *Quantum Electron.* **2018**, *48*, 438–442. [[CrossRef](#)]
26. Das, D.; Natarajan, V. Absolute frequency measurement of the lithium D lines: Precise determination of isotope shifts and fine-structure intervals. *Phys. Rev. A* **2007**, *75*, 052508. [[CrossRef](#)]
27. Magnus, F.; Boatwright, A.L.; Flodin, A.; Shiell, R.C. Optical pumping and electromagnetically induced transparency in a lithium vapour. *J. Opt. B Quantum Semiclassical Opt.* **2005**, *7*, 109–118. [[CrossRef](#)]
28. Saakyan, S.A.; Sautenkov, V.A.; Zelener, B.B. Long-term frequency stabilized and linewidth-narrowed cw-laser system for excitation of lithium Rydberg states. *J. Phys. Conf. Ser.* **2018**, *946*, 012128. [[CrossRef](#)]
29. Robertson, E.J.; Šibalić, N.; Potvliege, R.M.; Jones, M.P.A. ARC 3.0: An expanded Python toolbox for atomic physics calculations. *Comput. Phys. Commun.* **2021**, *261*, 107814. [[CrossRef](#)]
30. Raitzsch, U.; Heidemann, R.; Weimer, H.; Butscher, B.; Kollmann, P.; Löw, R.; Büchler, H.P.; Pfau, T. Investigation of dephasing rates in an interacting Rydberg gas. *New J. Phys.* **2009**, *11*, 055014. [[CrossRef](#)]
31. Singer, K.; Stanojevic, J.; Weidemüller, M.; Côté, R. Long-range interactions between alkali Rydberg atom pairs correlated to the ns–ns, np–np and nd–nd asymptotes. *J. Phys. B At. Mol. Opt. Phys.* **2005**, *38*, S295–S307. [[CrossRef](#)]

Disclaimer/Publisher’s Note: The statements, opinions and data contained in all publications are solely those of the individual author(s) and contributor(s) and not of MDPI and/or the editor(s). MDPI and/or the editor(s) disclaim responsibility for any injury to people or property resulting from any ideas, methods, instructions or products referred to in the content.